Molecular Heterogeneity of *O*-Acetylserine Sulfhydrylase by Two-Photon Excited Fluorescence Fluctuation Spectroscopy

Giuseppe Chirico,* Stefano Bettati,†‡§ Andrea Mozzarelli,†§ Yan Chen,¶ Joachim D. Müller,¶ and Enrico Gratton¶

*Istituto Nazionale per la Fisica della Materia, Università di Milano-Bicocca, Milano 20133, Italy; †Istituto di Scienze Biochimiche, ‡Istituto di Scienze Fisiche e §Istituto Nazionale per la Fisica della Materia, Università di Parma, Parma 43100, Italy; and ¶Laboratory for Fluorescence Dynamics, University of Illinois at Urbana-Champaign, Urbana, Illinois 61801 USA

ABSTRACT *O*-acetylserine sulfhydrylase, a homo-dimeric enzyme from *Salmonella typhimurium*, covalently binds one pyridoxal 5′-phosphate molecule per subunit as a fluorescent coenzyme. Different tautomers of the Schiff base between the coenzyme and lysine 41 generate structured absorption and fluorescence spectra upon one-photon excitation. We investigated the protein population heterogeneity by fluorescence correlation spectroscopy and lifetime techniques upon two-photon excitation. We sampled the fluorescence intensity from a small number of molecules (~10) and analyzed the distribution of photon counts to separately determine the number and the fluorescence brightness of excited protein molecules. The changes in the average number of molecules and in the fluorescence brightness with the excitation wavelength indicate the presence of at least two fluorescent species, with two-photon excitation maxima at 660 and 800 nm. These species have been identified as the enolimine and ketoenamine tautomers of the protein-coenzyme internal aldimine. Their relative abundance is estimated to be 4:1, whereas the ratio of their two-photon cross sections is reversed with respect to the single-photon excitation case. Consistent results are obtained from the measurement of the lifetime decays, which are sensitive to the excited-state heterogeneity. At least two components were detected, with lifetimes of ~2.5 and 0.5 ns. The lifetimes are very close to the values measured in bulk solutions upon one-photon excitation and attributed to the ketoenamine tautomer and to a dipolar species formed upon proton dissociation in the excited state.

INTRODUCTION

Recent years have seen significant advances in the optical characterization of single molecules in condensed environments (Moerner and Orrit, 1999). With such studies the heterogeneity of the molecular system can be characterized and related to the microenvironment. Moreover, the application of nonlinear fluorescence excitation has provided new methods to greatly simplify the excitation of small volumes (Denk et al., 1990) while avoiding photobleaching of the bulk solution.

The experimental effort to achieve a resolution close to the single-molecule level is fully rewarded whenever the heterogeneity of the system is strictly related to its function, and is otherwise buried in the averaged responses obtained through conventional ensemble measurements. In the case of proteins, spectroscopic heterogeneity often arises from the co-presence of molecules with different conformational states and/or different electronic states of bound chromophoric cofactors. In the present study we investigated the heterogeneity of the spectroscopic response of a globular protein, *O*-acetylserine sulfhydrylase, by measuring the fluorescence fluctuations and the lifetime of the protein cofactor. The tiny excitation spots needed for the excitation of a small number of molecules were obtained by means of two-photon excitation fluorescence.

O-acetylserine sulfhydrylase-A from *Salmonella typhimurium* (OASS; E.C. 4.2.99.8; http:/www.rcsb.org; PDB entry 10AS) (Becker et al., 1969) catalyzes the synthesis of L-cysteine from *O*-acetylserine and sulfide in enteric bacteria. The enzyme is a homo-dimer, each subunit having a mass of 34,450 Da (Levy and Danchin, 1988). In the absence of substrates or catalytic products, one molecule of the coenzyme pyridoxal 5′-phosphate (PLP) is covalently bound to each subunit via a Schiff base formed with the side chain of lysine 41 (Rege et al., 1996). This species, the internal aldimine (Christen and Metzler, 1985), exhibits a visible absorbance spectrum characterized by a main band peaked at 412 nm and a weak shoulder at ~330 nm (Fig. 1). These two bands have been attributed to the ketoenamine and enolimine tautomers of the bound coenzyme, respectively (Scheme 1) (Becker et al., 1969; Schnackerz et al., 1995; Benci et al., 1999). The equilibrium between the two tautomers depends on the active site polarity, the enolimine being favored by a more hydrophobic microenvironment (Arrio-Dupont, 1970; Kallen et al., 1985; Schnackerz et al., 1995). The relevance of the two isomers for the enzymatic activity has not been determined, mainly because the rate of catalysis is slower than the tautomer interconversion. Because the interconversion of the two tautomers is slower than the actual proton transfer reaction, a conformational change is probably associated with the isomerization (Faeder and Hammes, 1970). As many other PLP-dependent proteins, OASS has been shown to adopt alternative conformations along the catalytic pathway: closed, catalytically

Received for publication 16 June 2000 and in final form 29 December 2000.

Address reprint requests to Dr. Giuseppe Chirico, Universita di Milano-Bicocca, Istituto Nazionale pe la Fisica della Materia, Via Celoria 16, Milano 20133, Italy. Tel.: 39-02-2392355; Fax: 39-02-2392482; E-mail: giuseppe.chirico@mi.infm.it.

0006-3495/01/04/1973/13 $2.00

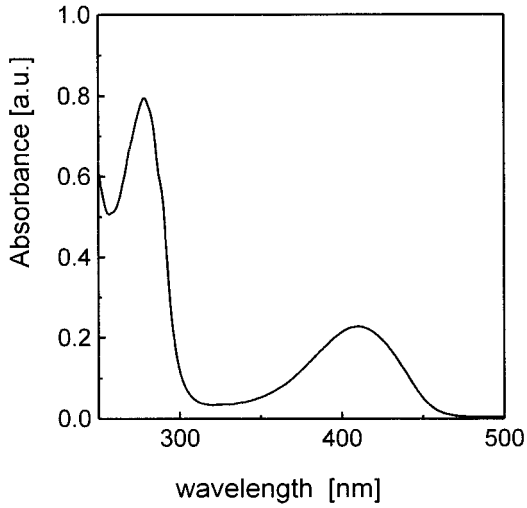

FIGURE 1 Absorbance spectrum of OASS. Enzyme protomers concentration was 29.9 μM in 100 mM potassium phosphate, pH 7.

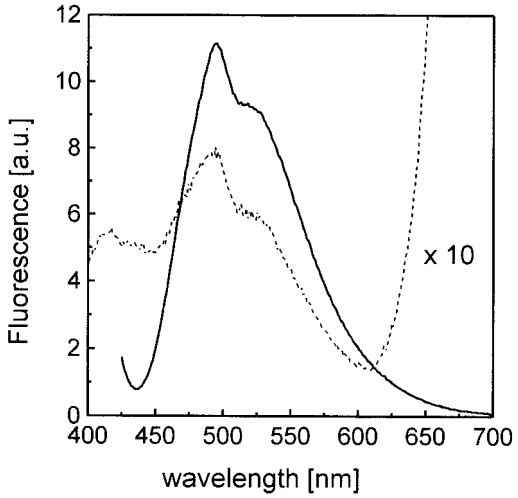

FIGURE 2 Emission spectra of 12 μM (protomers) OASS in 100 mM potassium phosphate, pH 7, upon one-photon excitation at 330 nm (— — —) or 412 nm (——). For clarity, the reported fluorescence intensity upon excitation at 330 nm has been multiplied 10-fold.

active conformations and open conformations (inactive). The internal aldimine of OASS is in an open conformation (Burkhard et al., 1998), likely favoring a more polar microenvironment within the active site cleft.

Upon excitation at 330 nm the OASS internal aldimine exhibits a weak fluorescence and a structured emission spectrum (Fig. 2). The main band at 490 nm and the shoulder at 420 nm are due to the ketoenamine and enolimine tautomers, respectively, indicating that an enolimine-to-ketoenamine (not directly excited at 330 nm) isomerization occurs in the excited state (Benci et al., 1999). The second shoulder at ~530 nm has been attributed to another excited-state reaction leading to the formation of a dipolar species upon Schiff base imine proton dissociation (Benci et al., 1999). The deprotonated species is not directly excited, and the same excitation pattern is found when emission is monitored at 490 or 530 nm (Benci et al., 1999). OASS emission intensity is much higher upon direct excitation of the ketoenamine tautomer at 412 nm and still shows a structured spectrum with a maximum at 490 nm and a pronounced shoulder at ~530 nm (Fig. 2).

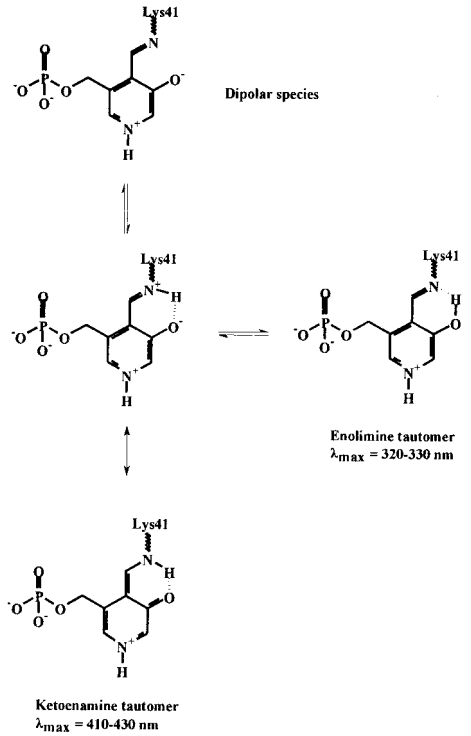

Scheme 1

The fluorescence lifetimes of OASS internal aldimine tautomers have been estimated from time-resolved fluorescence data upon excitation at 330 and 412 nm and species associated spectra upon excitation at 350 nm (Benci et al., 1999). Lifetime multifrequency phase and modulation data upon laser excitation at 350 nm (Benci et al., 1999) are well described by three-exponential decays with lifetimes $\tau_1 \cong 0.5$ ns, $\tau_2 \cong 2.4$, ns and $\tau_3 \cong 7$ ns with very similar fractional intensities. The fractional contribution of the slower component decreases on the red side of the emission spectrum. This supports its attribution to the enolimine tautomer. Upon excitation at 412 nm (Benci et al., 1999) or 454 nm (Bettati et al., manuscript in preparation), only the intermediate and fast component (attributed to the ketoenamine and its deprotonated form, respectively) are detected. The latter is more populated on the red side of the emission spectrum and when the excitation is performed at 454 nm.

In the present study we exploited the two-photon excitation of the internal aldimine of OASS to measure the fluorescence photon-counting histogram (PCH) arising from a small (~0.15 fl) volume of micromolar protein solutions.

We also used two-photon excitation to determine the fluorescence lifetime of the protein-coenzyme complex under the same experimental conditions. The analysis of the PCHs collected for different excitation wavelengths by a method recently developed (Chen et al., 1999) yields the number of protein molecules in the excitation volume $\bar{N}$ and the molecular brightness, ϵ. Other groups have recently described the same approach to extract information from the distribution of photon counts (Kask et al., 1999, 2000; Bieschke et al., 2000). Our results indicate that, when a single component is assumed, the average number of OASS molecules in the excitation volume changes with the excitation wavelength at a significantly higher extent than that expected from the change of the excitation volume with wavelength. This result indicates, at the single-molecule resolution, that at least two differently absorbing forms of the protein are simultaneously present in solution. The wavelength dependence of the average number of proteins in the excitation volume and of its fluorescence yield is then analyzed by taking into account a two-component character of the sample. We correlate the results of the PCH analysis with the lifetime measurements. This allows us to estimate the relative amount of the different protein species present. Moreover, by correlating the PCH to the lifetime measurements we detected differences in the protein tautomer distribution in the ground and excited state.

Fluorescence fluctuation spectroscopy

Fluorescence fluctuation spectroscopy is a very sensitive tool to investigate a variety of phenomena, from translational and rotational diffusion to chemical reactions (Elson and Magde, 1974; Magde and Elson, 1974; Ehrenberg and Rigler, 1974; Aragon and Pecora, 1976). Confocal detection is usually adopted to achieve very small excitation volumes (Qian and Elson, 1991; Rigler et al., 1993; Koppel et al., 1994) with low-power continuous wave (CW) laser sources. More recently two-photon (and multi-photon) excitation with pulsed infrared lasers has been exploited to enhance the background rejection and eliminate photobleaching outside from the focal regions. In both cases, the time dependence of fluorescence has been widely characterized by time-correlation methods. The analysis of the autocorrelation function (ACF) of the fluorescence signal as detected by a photomultiplier (PMT) or an avalanche photodiode (APD) gives two main parameters, the average number of molecules in the excitation volume, $\bar{N}$, and the molecular translational diffusion coefficient, D. The latter is related to the molecular radius, R, the solution temperature, T, and viscosity, η, by the Einstein relation: $D = k_B T/6\pi\eta R$. Beside the correlation functions, the probability distribution of the photon counting is used to describe random processes (Saleh, 1978), although it has generally received less attention. Recently, a theoretical and experimental study (Chen et al., 1999; Kask et al. 2000; Bieschke et al., 2000) has shown how to extract from the PCH detailed information on the average number of molecules, $\bar{N}$, and the molecular brightness, ϵ. The molecular brightness ϵ describes the detected fluorescence photon rate of a single molecule. This theoretical treatment of the photon count distribution implements the previous ones (Qian and Elson, 1990, 1989) by taking explicitly into account the shape of the point spread function and the motion of the tracer molecules. The experimental tests proved that this approach can be effectively applied to quantitatively resolve a mixture of species characterized by different molecular brightness values (Muller et al., 2000). The single-molecule PCH $p^{(1)}(k, V_0, \epsilon)$ is the probability of measuring k photon counts from a single tracer molecule in the volume V_0 (Chen et al., 1999). For integration times much smaller than the fluctuation time of the fluorescence emission this function is given by (Chen et al., 1999):

$$p^{(1)}(k, \epsilon, V_0) = \frac{1}{V_0}\int_{V_0} \frac{(\epsilon W(\mathbf{r}))^k e^{-\epsilon W(\mathbf{r})}}{k!}\, d\mathbf{r}, \qquad (1)$$

where ϵ is the molecular brightness of the tracer molecule given by the product of the photon detector (PMT or APD) quantum efficiency, instrumental factors, the molecular excitation probability, and the fluorescence yield. The energy distribution in the object plane is described by the function $W(\mathbf{r})$.

The PCH in an open system should not depend on the particular choice of the sampling volume in Eq. 1, and following the convention used in fluorescence correlation spectroscopy (Chen et al., 1999), we chose $V_0 \int W(\mathbf{r}) d\mathbf{r}$. The PCH of a single molecule is given by Eq. 15 in Chen et al. (1999) for a Gaussian-Lorentzian beam profile W(r). For a solution with a molar concentration C the measured PCH, $\Pi(k, \bar{N}, \epsilon)$ is given by a convolution over all the possibilities of getting a total of k photon counts averaged over the Poissonian number distribution of molecules (Chandrasekhar, 1943):

$$\Pi(k, \bar{N}, \epsilon) = \sum_{N=0}^{\infty} p^{(N)}(k, V_0, \epsilon) \frac{\bar{N}^N e^{-N}}{N!}, \qquad (2)$$

where

$$p^{(N)}(k, V_0, \epsilon) = \left(\underbrace{p^{(1)} \otimes \ldots \otimes p^{(1)}}_{N \text{ times}}\right)(k, V_0, \epsilon) \qquad (3)$$

The average number of molecules in the reference volume V_0, $\bar{N} = CV_0N_{av}$, is proportional to Avogadro's number, N_{av}, and the sample molar concentration, C.

It should be noticed that for a single chemical species the average number of molecules $\bar{N}$ is supposed to be independent of the excitation wavelength, whereas the molecular brightness ϵ should vary as a function of wavelength. In fact, the wavelength dependence of ϵ, once corrected for wavelength-dependent changes in the excitation intensity, is proportional to the two-photon absorption spectrum of the tracer molecule.

Gratton and co-workers (Chen et al., 1999) have shown that the PCH of a mixture of two species with molecular brightness values ϵ_1 and ϵ_2 is given by a convolution of the PCH functions of each species:

$$\Pi(k, \bar{N}_1, \bar{N}_2, \epsilon_1, \epsilon_2) = \sum_{h=0}^{k} \Pi(h, \bar{N}_1, \epsilon_1)\Pi(k-h, \bar{N}_2, \epsilon_2) \quad (4)$$

The molecular brightness ϵ is proportional to the fluorescence quantum yield ϕ, the wavelength-dependent two-photon cross section $\alpha(\lambda)$, and the square of the excitation intensity $I_0(\lambda)$, as $\epsilon(\lambda) \propto \alpha(\lambda)I_0^2(\lambda)\phi$.

Let us consider as an example the case of two species with average particle numbers $\bar{N}_1$ and $\bar{N}_2$. We assume that the two species have non-overlapping spectra centered at wavelengths λ_1 and λ_2, with $\epsilon_1(\lambda_2) \cong 0$ and $\epsilon_2(\lambda_1) \cong 0$. In this limiting case, the analysis of the PCH measured at λ_1 and λ_2 reduces to the single-species case and simply yields the average number of molecules $\bar{N}_1$ and $\bar{N}_2$, respectively. If the spectra partially overlap, a detailed analysis of the PCH measured at an intermediate wavelength λ would give, in principle, $\bar{N}_1$, $\bar{N}_2$, $\epsilon_1(\lambda)$, and $\epsilon_2(\lambda)$. The average number of molecules, $\bar{N}_1$ and $\bar{N}_2$, is wavelength independent. However, if the molecular brightness values of the two species are rather small, the signal statistics of the experimental PCH is not sufficient to directly resolve both species (Müller et al., 2000). Under these circumstances the experimental PCH is satisfactorily analyzed in terms of a single-species PCH (see Eq. 2). Of course, the fit parameters do not reflect the actual brightness and particle concentration of the mixture, but rather yield an apparent molecular brightness, ϵ_{app}, and an apparent particle number, $\bar{N}_{app}$, which are functions of $\epsilon_1(\lambda)$, $\epsilon_2(\lambda)$, $\bar{N}_1$, and $\bar{N}_2$. Thus, the number $\bar{N}_{app}$, in contrast to $\bar{N}_1$ and $\bar{N}_2$, depends on the excitation wavelength. In the Discussion we will illustrate how we solve the apparent fit parameters into individual molecular species via a global fitting approach.

MATERIALS AND METHODS

Instrumentation

The instrumentation for the two-photon fluctuation experiments is similar to that described by Berland et al. (1996) and Chen et al. (1999). All experiments were performed with a Zeiss Axiovert 135 TV microscope (Thornwood, NY) equipped with a Zeiss 40× Fluor oil immersion objective (N.A. 1.3). The excitation source was a mode-locked Ti:Sapphire laser (Mira 900, Coherent, Palo Alto, CA) pumped by a frequency-doubled Nd-Yag laser (Verdi 5W, Coherent). The excitation wavelength was varied in the range 740–805 nm and the estimated power at the sample ranged from 10 to 25 mW. The fluorescence and excitation light were discriminated by a Chroma Technology (Brattelboro, VT) dichroic mirror centered around 750 nm and by a BG39 (Chroma Technology) short-pass filter. For the measurements of the fluorescence fluctuations the photon counts were detected through the bottom port of the microscope by an APD (SPCM-AQ-151, EG&G, Wellesley, MA). The TTL digital output of the APD is fed to a home-built acquisition board (Eid et al., 2000) and stored in the computer memory. The acquisition sampling frequency was always set at 20 kHz, and the stored photon counting files were analyzed with programs written with the PV-WAVE software, version 6.10 (Visual Numerics, Houston, TX).

For the lifetime measurements, the fluorescence light was detected through the front port of the microscope by a photomultiplier (R928, Hamamatsu, Bridgewater, NY) whose gain was modulated by biasing the second dynode stage at a radio frequency ν + 800 Hz, with ν = 80, 160, 240, and 320 MHz. The PMT signal, after amplification through a low-noise current amplifier (SR570, Stanford Research, Sunnyvale, CA), was fed to an ISS board (ISS, Champaign, IL) for the computation of the modulation ratios and phase differences of the fluorescence light with respect to the excitation laser beam. The synchronization was performed by a Synchro-lock 900 system (Coherent), taking as a reference the signal of a fast diode that detects a small portion of the laser light. The 10-MHz output of the synchro-lock was used by three Hewlett-Packard (Palo Alto, CA) frequency synthesizers to give 1) the 1.024-MHz clock for the ISS board, 2) an analog output simulating the reference PMT input for the ISS board, and 3) the radio-frequency bias for the modulation of the gain of the PMT.

Absorbance spectra were recorded using a Perkin-Elmer (Wellesley, MA) Lambda 40 UV/visible spectrophotometer, and the buffer absorption was subtracted. Emission spectra upon one-photon excitation were recorded using a phase fluorometer (GREG 200, ISS), and the fluorescence intensity of the solvent was subtracted. Excitation and emission slits of the monochromators were 1 nm.

Sample preparation

O-acetylserine sulfhydrylase (A-isozyme) was prepared from a plasmid-containing *Salmonella typhimurium* overproducing strain (LT-2) according to the method of Hara et al. (1990), modified by Tai et al. (1993), and was a kind gift of Dr. Paul F. Cook (Department of Chemistry and Biochemistry, University of Oklahoma, Norman, OK). The enzyme concentration was estimated on the basis of an extinction coefficient of 7600 M^{-1} cm^{-1} at 412 nm for protomers (Becker et al., 1969). A buffer solution containing 100 mM potassium phosphate, pH 7.0, was used.

Rhodamine 110 and fluorescein were purchased from Molecular Probes (Eugene, OR). Rhodamine concentration for FCS experiments was 11 nM in 50 mM Tris[hydroxymethyl]amino-methane (Sigma Chemical Co., St. Louis, MO), and the pH was adjusted to 8.5 with HCl. Fluorescein samples for the lifetime measurements were 120 nM in dilute NaOH solution.

Data analysis

Photon-counting histogram

The data analysis was performed by fitting Eq. 2 to the normalized experimental PCH as described by Chen et al. (1999). In the present study the PCHs are computed on collections of $M \cong 10^7$ data points and the normalized histogram value $p_{exp}(k)$ varies over several orders of magnitude. The different points of the histogram are weighed according to a binomial distribution, as given by Eq. 27 in Chen et al. (1999). The background contribution was estimated by measuring the photon count distribution of the buffer alone. This is well approximated by a Poisson distribution with an average of ~100 cps. The background contribution was taken into account in the fitting by convoluting Eq. 2 with the Poisson function of the background. Single (Eq. 2) species analyses were performed on the experimental PCH. The excitation volume was measured from the analysis of the autocorrelation functions at λ_{ex} = 770 nm and was determined as $V_0 = \int W(\mathbf{r})d\mathbf{r} = 0.15 \pm 0.01$ fl. From the equation $\int W(\mathbf{r})d\mathbf{r} = \pi w^4/\lambda$ we could estimate a beam waist $w \cong 0.44$ μm. Because the beam waist depends linearly on the wavelength, the use of different excitation wavelengths in the range $740 < \lambda < 805$ nm corresponds to a variation of ~±11% of the excitation volume.

Autocorrelation functions

The fluorescence temporal characteristics were analyzed by computing the autocorrelation function (ACF) of the detected signal. If $k(t)$ is the number of detected photon counts at time t, the correlation function is computed as $g_F(\tau) = \{\langle k(t + \tau)k(t)\rangle_t - \langle k(t)\rangle_t^2\}/\langle k(t)\rangle_t^2$. The subscript t indicates the average over the whole acquisition period. The ACF functions were analyzed according to a model introduced by Berland et al. (1996) that allows the determination of the protein diffusion coefficient D.

Lifetime analysis

The modulation $\Lambda(\nu)$ and phase shifts $\Delta(\nu)$ were measured at various harmonics of the repetition frequency of the Ti-sapphire laser. A 120 nM fluorescein solution in diluted NaOH (4.05 ns) was used as lifetime standard reference. The modulation and phase shift data were fitted to a single- or double-exponential decay scheme using the Globals Unlimited software (Beechem and Gratton, 1988).

RESULTS

Measurements of fluorescence fluctuations at $\lambda_{ex} = 775$ nm as a function of the excitation power

The wavelength dependence of the laser output power in the range 745 nm $< \lambda <$ 805 nm affects the shape of the measured PCH, because the apparent molecular brightness depends on the excitation intensity. To correct the PCHs for the variations of the laser power we characterized the response of rhodamine 110 and OASS solutions at a fixed wavelength (775 nm) as a function of the excitation power in the range 4–24 mW (at the sample plane). The fluorophore concentration was 11 nM for rhodamine 110 and 1.2 μM for OASS. This corresponds to an average number of molecules in the excitation volume of ~1.3 and ~140 for rhodamine and protein (protomers), respectively. The total fluorescence photon rate was in the range 2–70 kHz for both samples.

Typical PCHs and the respective fits are reported in Fig. 3. The PCH of rhodamine solutions is satisfactorily described by a single-component analysis, as can be seen from the residuals in the lower panel of Fig. 3. It is very unlikely that the nonrandom behavior of the residuals is due to the presence of more than one fluorescent component. This nonrandom feature is in fact observed for both the rhodamine (expected to exhibit a single fluorescent component) and OASS solutions. The brightness of the protein is too low to allow the discrimination of more than one component from the PCH analysis (see Discussion). The nonrandom behavior of the residuals, which are all within the uncertainty of the PCH, might instead be due to minor setup misalignments, inducing a slight deformation of the energy distribution $W(\mathbf{r})$ (see Eq. 1). We have verified the soundness of this hypothesis by numerical simulations (data not shown). Therefore, we consider hereafter a single-component analysis of the PCH.

The analysis according to a single-species model (Eq. 2) of the PCHs for OASS solutions gives reasonable results.

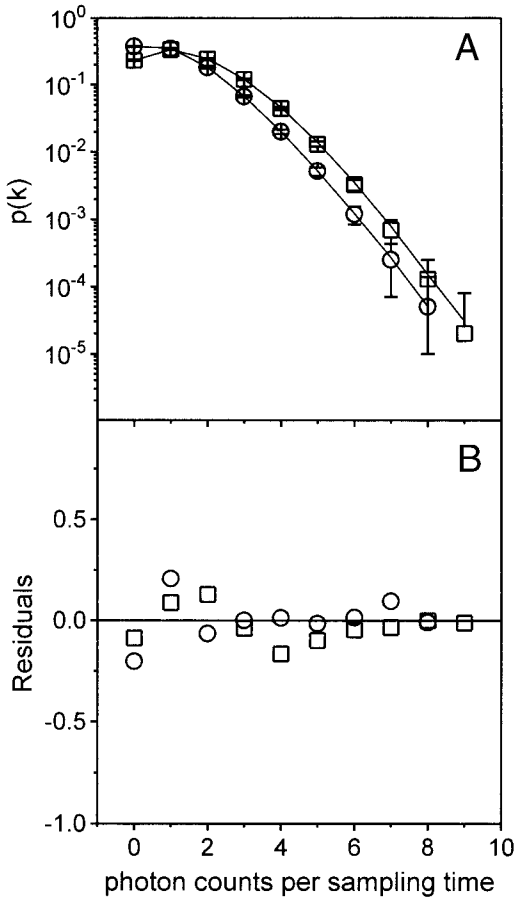

FIGURE 3 PCHs for a 1.2 μM OASS solution in 100 mM potassium phosphate, pH 7 (□) and for an 11 nM rhodamine 110 solution in 50 mM Tris[hydroxymethyl]amino-methane, pH 8.5 (○). The excitation wavelength was 775 nm, the excitation power ≅ 20 mW. The sampling time was 50 μs. (*A*) Single species best fit for OASS and rhodamine solutions (——). (*B*) Residuals (the difference between the experimental and the best fit PCHs divided by the PCH uncertainty) are shown for the OASS (□) and rhodamine solutions (○).

The apparent average number of molecules and fluorescence yield, indicated here as $\langle N\rangle$ and $\langle\epsilon\rangle$, are reported in Fig. 4 for rhodamine 110 and in Fig. 5 for OASS. In Fig. 4 *B* we also report the average fluorescence rate for rhodamine 110, together with a best fit to a square law. The contribution of the background counts to the fluorescence signal is always less than 5%. The constancy of $\langle N\rangle$ and the square law dependence of $\langle\epsilon\rangle$ on the excitation power (Figs. 4 and 5) indicate that any photobleaching effect is negligible in our experimental conditions.

Measurements of fluorescence fluctuation as a function of the excitation wavelength

PCHs have been collected at different excitation wavelengths, in the range 745–805 nm, for both OASS and rhodamine 110. At each wavelength, at least three measure-

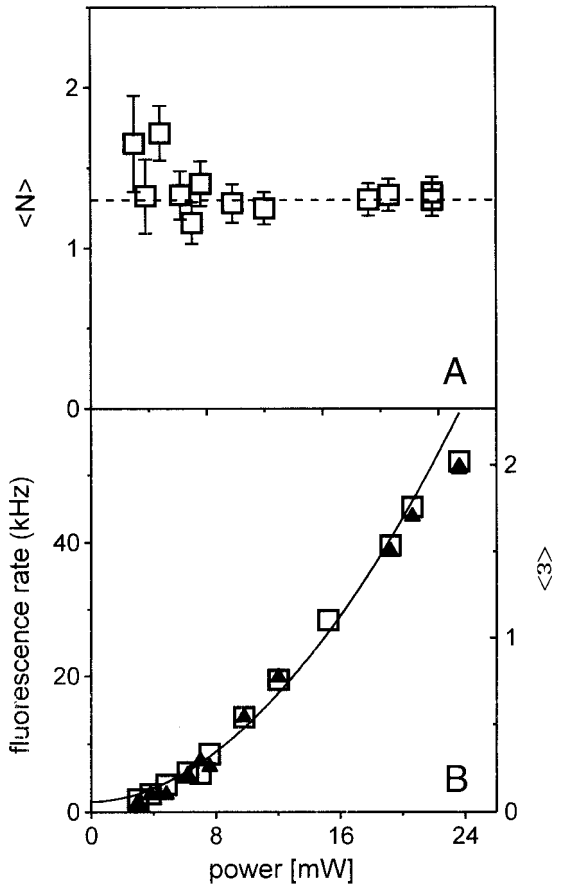

FIGURE 4 Results of the fit of the PCHs for 11 nM rhodamine 110 in 50 mM Tris[hydroxymethyl]amino-methane, pH 8.5. The average number of molecules, $\langle N \rangle$ (*A*), the average molecular brightness, $\langle \epsilon \rangle$, for a sampling time of 50 μs (*B*, right axis, ▲), and the average fluorescence rate, *F* (*B*, left axis, □) are reported as a function of the excitation power at $\lambda_{ex} = 775$ nm. The dashed line in *A* indicates the average number of rhodamine molecules, 1.3 ± 0.1. The solid line in *B* is a square law fit of the fluorescence yield.

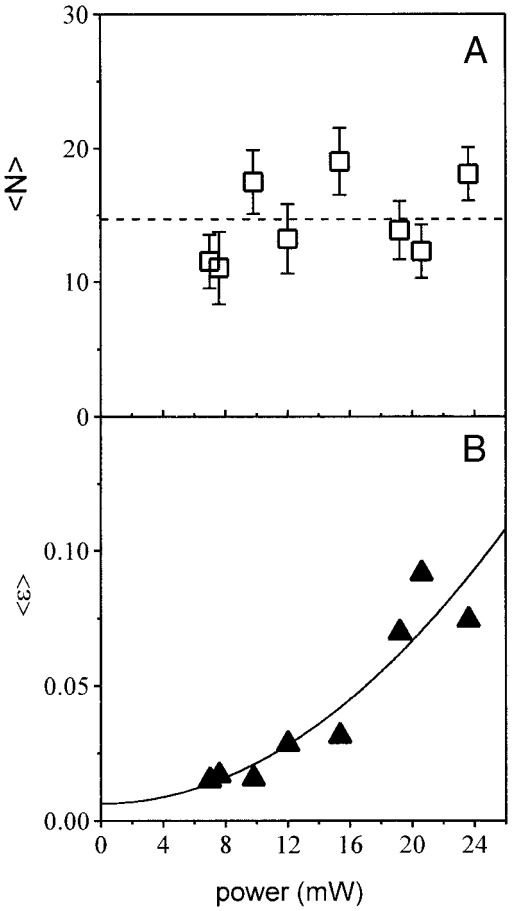

FIGURE 5 Fit of the PCHs for 1.2 μM OASS in 100 mM potassium phosphate, pH 7. The average number of molecules, $\langle N \rangle$ (*A*), and the molecular brightness, $\langle \epsilon \rangle$, for a sampling time of 50 μs (*B*), are reported as a function of the excitation power at $\lambda_{ex} = 775$ nm. The dashed line in *A* indicates the average number of OASS molecules, 15 ± 3. The solid line in *B* is a square law fit of the fluorescence yield.

ments of the protein and the rhodamine solutions were performed. The systematic changes of the excitation power with wavelength were monitored with a power meter and appeared to vary in accordance with the laser data sheet. The spectral line-width of the laser was checked at each wavelength and was found to be 8 ± 1 nm in all cases. The single-species analysis has been applied to the PCHs collected from the rhodamine and the OASS solutions. The recovered average number of proteins per excitation volume, $\langle N \rangle$, is shown in Fig. 6 together with the wavelength dependence of the excitation power (Fig. 6, *inset*). In the case of rhodamine we observed no large changes of $\langle N \rangle$ as a function of wavelength. The calculated value of $\langle N \rangle$ for rhodamine 110 is 1.3 ± 0.06, which, assuming $V_{PSF} = 0.15 \pm 0.01$ fl as previously determined (see Materials and Methods), corresponds to a concentration of 14 ± 1.2 nM, in good agreement with the nominal value, 11 nM. Over the wavelength range studied an overall increase of V_{PSF} by 23% is expected, because V_{PSF} scales as λ^3, as also verified on the autocorrelation functions of rhodamine solutions (see below). Therefore, the average number of rhodamine molecules within the excitation volume should depend on the excitation wavelength. Indeed, we observe a minor systematic change of $\langle N \rangle$ from $\lambda = 745$ nm where $\langle N \rangle \cong 1.2$ to $\lambda = 805$ nm where $\langle N \rangle \cong 1.4$ corresponding to ~17% increase. Because no dependence of the average number of molecules on the excitation intensity was observed in the investigated power range (Figs. 4 and 5), corrections for the varying laser power are not necessary for the data presented in Fig. 6.

The analysis of the PCHs of OASS and rhodamine 110 also provides the average molecular brightness, $\langle \epsilon \rangle$. In Fig. 7 we report the molecular brightness for OASS, which was corrected for the quadratic dependence on the excitation power (see Fig. 5). The apparent molecular brightness is shown together with the average fluorescence rate measured by the acquisition board.

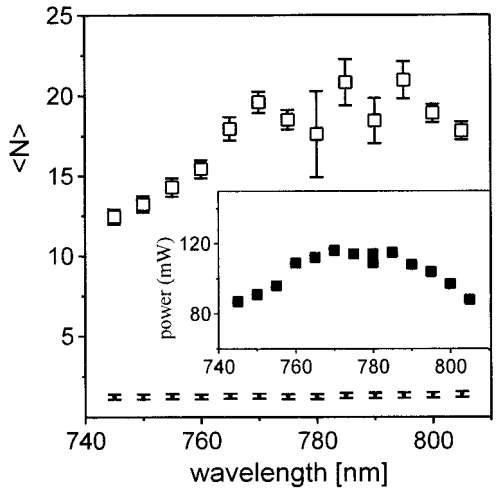

FIGURE 6 Dependence on the excitation wavelength of the average number of molecules per excitation volume, $\langle N \rangle$, as obtained from the best fit of PCHs for OASS (□) and rhodamine 110 (●). For sample concentration and buffers see captions to Figs. 3–5. (*Inset*) Wavelength dependence of the excitation power measured at the entrance of the microscope.

Measurements of the fluorescence lifetimes

The demodulation ratios and the phase shifts of the fluorescence light were measured at the modulation frequencies 80, 160, 240, and 320 MHz for each of the excitation wavelengths used for the fluorescence fluctuation measurements. To increase the average fluorescence signal, a concentration of 12 μM OASS was used. The lifetime reference was 120 nM fluorescein, which exhibits a single lifetime $\tau \cong 4.05$ ns in high-pH water solution (Tsien and Wagonner, 1995). The protein and fluorescein solutions were set in two adjacent wells of an eight-well glass slide (Nalge-Nunc, Naperville, IL). At each modulation frequency, 8–10 measurements were taken alternatively on the sample and reference solution by manually adjusting the microscope stage. Phase and modulation lifetimes were monitored during the measurements and were found to be significantly different, suggesting a multi-component fluorescence decay for OASS. The multi-exponential character of the fluorescence decay was confirmed by a fit of the phase and modulation data to a single-species (solid line) and two-species (dashed line) model, as shown in Fig. 8 (for $\lambda_{ex} = 775$ nm). In Fig. 9 we report the dependence of the two measured lifetimes, τ_S and τ_F, and the relative fractional intensity, f_S and f_F, on the excitation wavelength.

Autocorrelation functions

Additional information on the system can be obtained from the autocorrelation function of the fluorescence photon counts. From the fit of the experimental ACFs of the rhodamine solutions to the theoretical curve (Berland et al., 1996), we obtain a beam waist $w_0 = 0.44 \pm 0.03$ μm at $\lambda_{ex} = 770$ nm, when a diffusion coefficient $D = 280$ $\mu m^2/s$ is assumed. The corresponding value of the excitation volume is $V_0 = 0.15 \pm 0.03$ fl at $\lambda_{ex} = 770$ nm (V_0 is found to scale as $\sim\lambda^3$). The best fit value of $g(0) = 0.09 \pm 0.01$ corresponds to a concentration of 9.1 ± 0.9 nM, in good agreement with the nominal concentration, 11 nM.

The ACFs (Fig. 10), computed for the OASS solutions on the same raw data used for the PCH analysis, are affected by larger experimental uncertainties than those of rhodamine, due to the relatively dim fluorescence of the OASS-PLP complex. Nevertheless, the result of the analysis of the ACFs is overall consistent with the theoretical predictions.

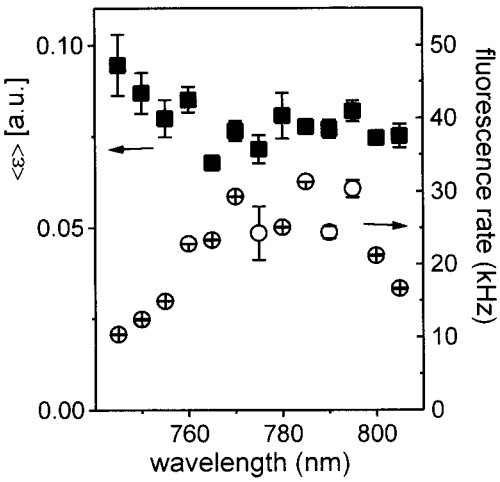

FIGURE 7 Apparent molecular brightness of OASS, $\langle \epsilon \rangle$ (■, left *y* axis), as obtained from the best fit of PCHs for 1.2 μM protein in 100 mM potassium phosphate, pH 7, as a function of the excitation wavelength. The average fluorescence rate is also shown (○, right *y* axis).

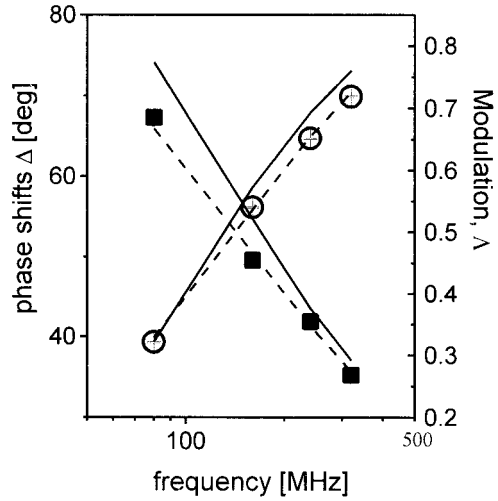

FIGURE 8 Phase shifts (○, left axis) and modulations (■, right axis), measured at $\lambda_{ex} = 775$ nm for a 12 μM OASS solution in 100 mM potassium phosphate, pH 7. The solid and dashed lines represent a single- and a two-species fit of the data.

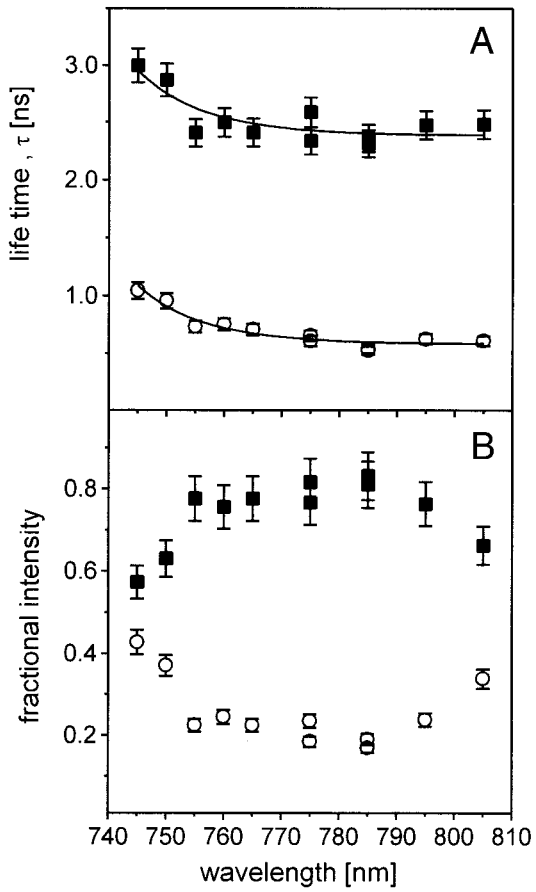

FIGURE 9 (*A*) Dependence on the excitation wavelength of the lifetimes of the slow (■) and fast (○) species. The solid lines are the best fit to an apparent relaxation time given by Eq. 10 as described in the text. (*B*) Fractional intensity of the two species. The symbols are the same as in *A*. The error bars indicate the standard deviation of each measurement.

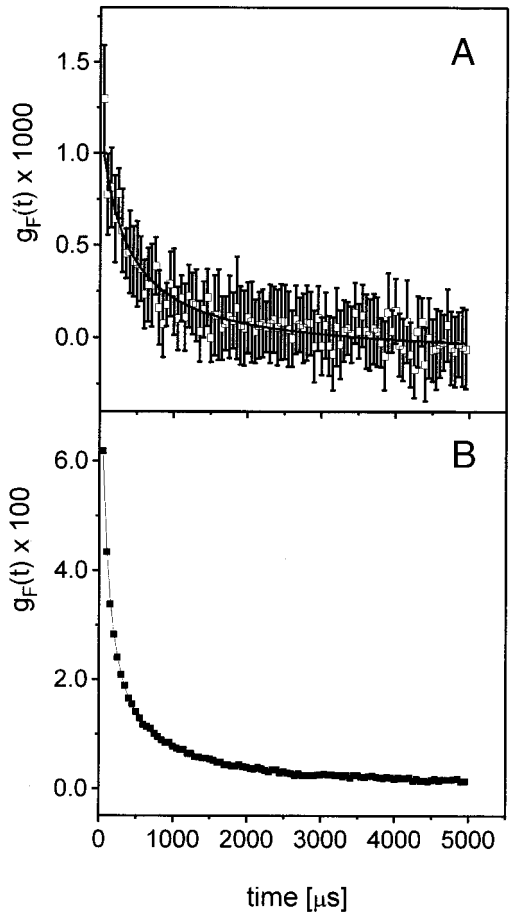

FIGURE 10 Autocorrelation function of the fluorescence measured at excitation wavelength λ_{ex} = 770 nm for OASS (*A*, □) and rhodamine 110 (*B*, ■) solutions. Rhodamine solution was 11 nM in 50 mM Tris[hydroxymethyl]amino-methane, pH 8.5. OASS was 1.2 μM (protomers concentration) in 100 mM potassium phosphate buffer, pH 7.0. The solid lines are the best fit to the theoretical correlation function introduced by Berland et al., 1996.

From the analysis of the ACFs of OASS we find a diffusion coefficient $D = 70 \pm 10$ $\mu m^2/s$, which corresponds to a protein average radius of 3 ± 0.7 nm. The radius that can be estimated for the protein, which is a dimer with molecular mass of 68,900 Da, is ~3.5 nm. This figure is obtained from the anhydrous radius of the protein monomer, ~2.2 nm, computed from the molecular weight and the partial molecular volume ~0.78 ml/g (Tanford, 1961). Changes to this value are made by taking into account that the dimer diffusion coefficient is decreased by ~33% due to the hydrodynamic interactions (Ermak and McCammon, 1978), it is increased by ~3% due to the protein anisotropy (the OASS dimer is an oblate ellipsoid with short axes ~4.5 nm and the longest axis ~8.5 nm) and that the hydration layer is typically ~0.3 nm. Considering the type of the previous assumptions, the agreement between the estimated and the experimental figure for the protein hydrodynamic radius is rather good. Our experimental estimate, $D = 70 \pm 10$ $\mu m^2/s$, is also confirmed by the direct computation of the protein diffusion coefficient, $D = 63$ $\mu m^2/s$, performed (De la Torre et al., 2000) on a continuous surface model of the protein structure. Finally, the protein concentration that is obtained from the measured value of $g(0) = 0.0016 \pm 0.006$ is 0.46 ± 0.2 μM, in agreement with the nominal concentration of OASS dimers in solution of ~0.6 μM. Altogether, the ACFs computed on the same amount of data collected for the PCH measurements are affected by larger statistical uncertainties than the histograms of the photon counting.

DISCUSSION

PCH analysis

A single-species model described the experimentally determined PCH of our samples within statistical error. The fit of each PCH determines an average molecule number, $\langle N \rangle$, and an apparent molecular brightness, $\langle \epsilon \rangle$. The number of rhodamine 110 molecules measured for excitation wavelengths ranging from 745 to 805 nm is approximately constant (Fig.

6), as expected for a single molecular species. In principle, the small change in the excitation volume upon varying the laser wavelength is expected to affect the average number of molecules, $\langle N\rangle$, and indeed a small ($\sim$17%) increase of $\langle N\rangle$ with λ is found. Different from rhodamine 110, an almost twofold change in the number of molecules is observed in the case of OASS, with a broad maximum at $\lambda_{ex} \cong 780-800$ (Fig. 6). The twofold increase of $\langle N\rangle$ for OASS as a function of the excitation wavelength suggests that the protein solution might consist of a heterogeneous population of molecules with different brightness properties.

Before exploring this hypothesis further, let us consider the fitting parameters of the PCH analysis. In the case of rhodamine 110 all molecules are accounted for by PCH analysis, because the calculated average number $\langle N\rangle = 1.3$ corresponds to a number concentration of $\sim$14 nM, which is very close to the nominal one (11 nM). On the contrary, the OASS concentration, as calculated from the PCH analysis, corresponds to 0.22 ± 0.07 μM, a value sensibly lower than the nominal one (0.6 μM OASS dimers). This suggests that a considerable fraction ($\sim$2/3) of OASS molecules in solution is either not excited by the infrared radiation or exhibits a very low molecular brightness. These findings are in substantial agreement with the analysis of the ACFs that give $C \cong 0.46 \pm 0.2$ μM.

The second parameter obtained from the analysis of the PCH is the molecular brightness $\langle\epsilon\rangle$, which depends on several molecular and instrumental parameters: the square of the excitation intensity, the two-photon cross section of the tracer molecules, and their fluorescence quantum yields. To correct the measured $\langle\epsilon\rangle$ for the variations in the excitation intensity as a function of wavelength, it is necessary to verify that the molecular brightness varies with the square of the excitation intensity in the investigated intensity range. We confirmed the quadratic power dependence of the molecular brightness $\langle\epsilon\rangle$ for rhodamine 110 (Fig. 4) and OASS (Fig. 5). In principle, corrections for the detector response at different emission wavelengths should also be applied, but rhodamine 110 and OASS emission occur in very similar spectral windows. Therefore, we corrected the measured $\langle\epsilon\rangle$ only for the variations of the excitation intensity.

Evidence for two spectroscopic species

After considering the influence of instrumental factors upon the PCH analysis, we resolved the heterogeneity of the OASS solutions from the excitation wavelength dependence of the apparent parameters $\langle N\rangle$ and $\langle\epsilon\rangle$ (see Figs. 6 and 7). This was carried out by assuming the presence of two species. First, we need to construct the mathematical relationship between the apparent fit parameters N_{app} and ϵ_{app} and the actual particle numbers and molecular brightness of the two species. By setting equal the first and the second moments of a single-species and of a double-species photon-counting distribution, one can derive an expression for N_{app} and ϵ_{app} in terms of the number of molecules N_1, N_2 and the fluorescence yield ϵ_1, ϵ_2 of the two species:

$$\begin{aligned} \langle k\rangle &= \epsilon_1 N_1 + \epsilon_2 N_2 = \epsilon_{app}\bar{N}_{app} \\ \frac{\langle k^2\rangle - \langle k\rangle^2}{\langle k\rangle^2} &= 1 + \gamma\frac{N_1\epsilon_1^2 + N_2\epsilon_2^2}{\epsilon_1 N_1 + \epsilon_2 N_2} = 1 + \gamma\epsilon_{app}, \end{aligned} \tag{5}$$

where the contrast factor γ is given by

$$\gamma = \frac{\int W^2(\mathbf{r})d\mathbf{r}}{\int W(\mathbf{r})d\mathbf{r}}. \tag{6}$$

The apparent number of fluorophores and the apparent molecular brightness are determined by Eqs. 5 and 6:

$$\begin{aligned} N_{app}(\lambda) &= \frac{(N_1\epsilon_1(\lambda) + N_2\epsilon_2(\lambda))^2}{(N_1\epsilon_1^2(\lambda) + N_2\epsilon_2^2(\lambda))} \\ \epsilon_{app}(\lambda) &= \frac{(N_1\epsilon_1^2(\lambda) + N_2\epsilon_2^2(\lambda))}{(N_1\epsilon_1(\lambda) + N_2\epsilon_2(\lambda))} \end{aligned} \tag{7}$$

Here we explicitly indicate the dependence of ϵ on the wavelength λ. This dependence may derive either from the two-photon cross section or from the emission spectrum. By using Eq. 7 we fit the apparent $\langle N\rangle$ and $\langle\epsilon\rangle$ of OASS (see Figs. 6 and 7) to two species with different molecular brightness, ϵ_1 and ϵ_2, with Gaussian wavelength dependence:

$$\epsilon_i(\lambda) = \frac{\epsilon_{i,0}}{(2\pi)^{0.5}\sigma_i}\exp[-(\lambda - \lambda_i)^2/(2\sigma_i^2)], \tag{8}$$

where $\epsilon_{i,0}$ is the molecular brightness of species i at the center of the Gaussian band located at the wavelength λ_i, and σ_i is the width of the band. The choice of Gaussian functions is suggested by the analysis of the single-photon absorption spectrum that can be fitted to the sum of two Gaussians in the range $300 < \lambda < 450$ nm (data not shown). We fit N_{app} and ϵ_{app} independently to our model. Both apparent parameters are well described by this model, as indicated in Fig. 11. The best-fit parameters are reported in Table 1, and the corresponding Gaussian components, $\epsilon_1(\lambda)$ and $\epsilon_2(\lambda)$, obtained by separately fitting $\langle N\rangle$ and $\langle\epsilon\rangle$, look very similar (Fig. 12). One of the two components is narrow and peaked around 800 nm, whereas the second is broader and peaked at $\sim$660 nm. Because the wavelength range investigated in the present study is 740–805 nm, the parameters associated with the 660-nm band are less well determined than those of the 800-nm band. The species corresponding to the component peaked at $\sim$800 nm is more populated, with $N_1/N_2 \cong 2.5-4$, based on the analysis of $\langle N\rangle$ and $\langle\epsilon\rangle$. It is noteworthy that the wavelengths of the two maxima of $\epsilon(\lambda)$, once divided by 2, well correspond to the single-photon excitation maxima of the ketoenamine ($\lambda_{max} \cong 412$ nm) and the enolimine ($\lambda_{max} \cong 330$ nm) tautomers of the OASS-coenzyme complex. Therefore, we

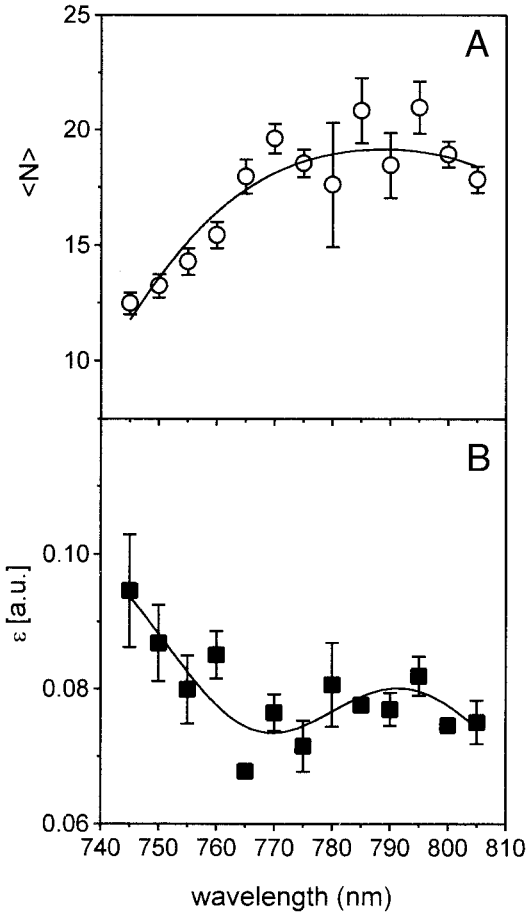

FIGURE 11 Dependence on the excitation wavelength of the apparent average number $\langle N \rangle$ of OASS molecules (*A*) and apparent molecular brightness ϵ (*B*), obtained from PCHs analysis. The solid lines are the best fit to Eqs. 7 and 8.

assume in the following that the short-wavelength band corresponds to the enolimine tautomer and the long-wavelength band represents the ketoenamine tautomer of the OASS-PLP Schiff base. The relative contribution to the fluorescence signal of each species was estimated from the products $\epsilon_{0i}N_i$ (Table 1). Because of the high $\epsilon_{2,0}/\epsilon_{1,0}$ ratio, the less populated component peaked at ~660 nm contributes four to five times more to the fluorescence signal than the component centered at ~800 nm, despite the larger number of OASS molecules excited at ~800 nm. As expected, no evidence for the dipolar species is found from the PCH analysis. The dipolar species occurs only in the excited state and is averaged with the ketoenamine species on the time scale of the PCH analysis (~50 μs).

TABLE 1 Best-fit parameters

	I	N_i	$\epsilon_{0,i}$ (a.u.)	λ_i (nm)	σ_i (nm)	$\epsilon_{0,i}$ N_i
From the fit of $\langle\epsilon\rangle$	1	11	4	793	23	44
	2	5	56	663	192	280
From the fit of $\langle N\rangle$	1	19	4	787	35	76
	2	4	60	660	180	240

Shown are results of fitting the wavelength dependence of the experimental particle number $\langle N\rangle$ and brightness $\langle\epsilon\rangle$ of OASS to two Gaussian components of the type: $\epsilon_i = \frac{\epsilon_{i,0}}{(2\pi)^{0.5}\sigma_i}\exp[-(\lambda - \lambda_i)^2/(2\sigma_i^2)]$. The first three rows summarize the analysis of the molecular brightness $\langle\epsilon\rangle$ whereas the last three rows represent the results of the analysis of $\langle N\rangle$.

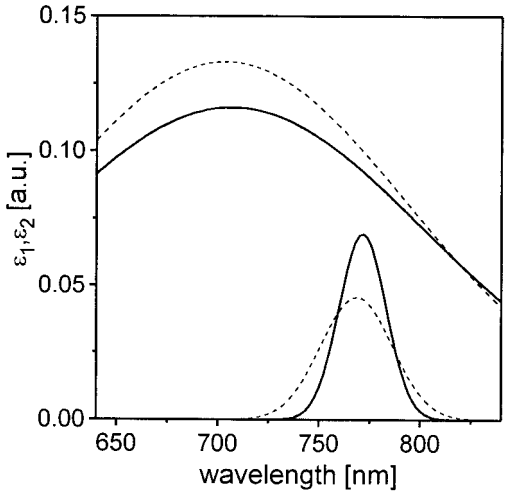

FIGURE 12 Gaussian components recovered from the fit of the average number of molecules $\langle N\rangle$ (— — —) and of the molecular brightness $\langle\epsilon\rangle$ (——) of OASS, based on Eqs.7 and 8.

The brightness factors $\epsilon_{1,0}$ and $\epsilon_{2,0}$ depend both on the fluorescence quantum yield and the two-photon cross section. To ascertain whether the higher value of $\epsilon_{2,0}$ is primarily due to a higher quantum yield or to a larger two-photon cross section one must take into account the differences in the emission properties. The molecular brightness, ϵ, is proportional to the two-photon cross section, α, and to the integral of the emission spectrum, *Em,* weighted by the collection efficiency of the optical setup. We assume here that the emission spectra upon single- or two-photon excitation are similar and take into account the corrections for the emission filter and the avalanche photodiode efficiency. We multiplied the emission spectra reported in Fig. 2 (extended to the region 350–700 nm) for the transmission spectrum of the BG39 filter and for the quantum efficiency of the APD. The ratio of the integrals of these corrected spectra has a value of ~16. This figure must be corrected also for the different single-photon absorption cross section at $\lambda = 330$ nm and $\lambda = 412$ nm and for the different excitation energy in the spectro-fluorometer used for the measurement of the emission spectra at $\lambda_{ex} = 330$ and 412 nm, which amounts to a factor of ~10. Therefore, the ratio of the brightness factors ϵ(ketoenamine)/ϵ(enolimine) $\cong$ 0.5 overestimates the ratio of the two-photon cross sections α(ketoenamine)/α(enolimine) by a factor of ~1.6, yielding α(ketoenamine)/α(enolimine) $\cong$ 0.3. Absolute values for the two-photon cross sections of the two tautomers

could be given referring to rhodamine 110. Unfortunately, we are not aware of measurements of the cross section of rhodamine 110 in water solution.

Regarding the PCH analysis, it would be obviously desirable to resolve the heterogeneity of the protein ensemble directly from the fitting of histograms. Unfortunately, the signal statistics of our protein sample prohibits such a direct evaluation of the problem. As a matter of fact, the fit of the OASS histograms with a single-species model satisfactorily describes the data (see Fig. 3), despite a nonrandom behavior of the residual that might be due to a slight misalignment of the setup. This result is due to the influence of signal statistics on the resolvability of species by the PCH method that was addressed recently (Müller et al., 2000). The ideal concentration range to resolve multiple species is close to a single particle in the excitation volume. Clearly, the protein concentration in our study was higher than the optimal one to be used for resolving multiple species. Had we used a lower concentration, the low fluorescence yield of the protein would prohibit anyway the resolution of multiple species. The data acquisition time necessary to build up the statistical accuracy required for the detection of two species can be determined through techniques used by Müller et al. (2000). Data acquisition times that exceed several days are estimated from this analysis, due to the low molecular brightness of OASS. Thus, to overcome the prohibitive long acquisition time, a global approach was used to resolve multiple species.

The measured lifetime was used to identify the coenzyme tautomers. The two observed lifetimes do not depend strongly on the excitation wavelength, and their average values, $\tau_S = 2.5 \pm 0.2$ ns and $\tau_F = 0.7 \pm 0.15$ ns (Fig. 9), are in good agreement with those for the ketoenamine tautomer ($\tau_K \cong 2.4$ ns) and the dipolar form of the PLP Schiff base ($\tau_D \cong 0.5$ ns) (Benci et al., 1999). Furthermore, as previously mentioned, the ketoenamine tautomer has a single-photon absorption maximum at 412 nm, in good agreement with the observed two-photon excitation at ~800 nm. Thus, we assign the slow and the fast lifetime component detected by two-photon excitation to the ketoenamine and its dipolar tautomer, respectively. It is noteworthy that the fractional intensities of the ketoenamine and the dipolar forms are in a ratio of 4 ± 1 for two-photon excitation at $\lambda \cong 770$ nm and in a ratio of ~2 and ~1.3 at $\lambda \cong 805$ nm and $\lambda \cong 745$ nm. Smaller ratios, ~1, have been found upon single-photon excitation (Benci et al. 1999). However, similarly to the present two-photon case, a decrease in the ratio of the fractional intensities is observed for single-photon excitation at wavelengths higher than the excitation peak. For example, the ratio of the fractional intensities that is ~1 at $\lambda = 412$ nm decreases to ~0.5 at $\lambda = 454$ nm.

No direct indication of a third component, corresponding to the enolimine form, is found in the lifetime spectra, which are satisfactorily described by a two-component model (see Fig. 8). It is possible that four modulation frequencies are not sufficient for the detection of the enolimine species as a third component. The enolimine species has a longer lifetime and probably a larger fluorescence quantum yield than the ketoenamine form (Benci et al., 1999) but the enolimine/ketoenamine number fraction estimated from the PCH analysis is only ~0.2–0.4. Still, we observe a modest but significant increase of both lifetimes for $\lambda < 750$ nm (Fig. 9). This finding is consistent with a small contribution from the long lifetime component. Let us assume, for example, a double-exponential fluorescence decay of the type:

$$f(t) = \frac{f_1(\lambda)}{\tau_1}\exp[-t/\tau_1] + \frac{f_2(\lambda)}{\tau_2}\exp[-t/\tau_2], \qquad (9)$$

where f_1, f_2 are the fractional intensities. If this decay is force-fitted to a single decay function, an effective relaxation time is obtained:

$$\frac{1}{\tau_{app}} = \frac{[f_1(\lambda)/f_2(\lambda)]\tau_1^{-2} + \tau_2^{-2}}{[f_1(\lambda)/f_2(\lambda)]\tau_1^{-1} + \tau_2^{-1}}. \qquad (10)$$

The wavelength dependence of the fractional intensity, $f(\lambda) \div N\epsilon(\lambda)$, is assumed to be the same as the one observed for $\epsilon(\lambda)$, and we fit each of the two measured lifetimes, τ_S and τ_F, to Eq. 10, in which one of the two fitting components is either the ketoenamine (for the component with $\tau \cong 2.5$ ns) or the dipolar species (for the component with $\tau \cong 0.5$ ns). The second fitting species should now have parameters very close to the enolimine tautomer (see Table 1). The solid lines in Fig. 9 *A* are the best-fit curves obtained by using the parameters λ_0 and σ of the Gaussian brightness spectra reported in Table 1 and leaving τ_1, τ_2, and the ratio f_1/f_2 as free parameters in Eq. 10. From the fitting of the slow lifetime component we obtain for the ketoenamine form $\tau_1 = \tau_k = 2.3$ ns, for the enolimine form $\tau_2 = \tau_E = 10$ ns, and $f_K/f_E \cong 1$. These findings are consistent with the analysis of the PCH. The population ratio of ketoenamine to enolimine species that can be predicted from the lifetime analysis is $N_K/N_E \cong (f_K\epsilon_E)/(f_E\epsilon_K)$. Because from the PCH measurements it is found that (see Fig. 12) the ratio $\epsilon_E/\epsilon_K \cong 2$, we can estimate $N_K/N_E \cong 2$, in reasonable agreement with the numbers obtained by PCH analysis. The fitting of the fast lifetime component yields $\tau_1 = \tau_D = 0.55$ ns for the dipolar form, $\tau_2 = \tau_E = 8$ ns for the enolimine form and $f_D/f_E \cong 0.08$. By taking into account the result of the analysis relative to the slow component, we obtain a ratio of $f_K/f_D \cong 12$, which again is substantially larger than the result of the single-photon studies, in which the fractional intensities of the ketoenamine, eneolimine, and dipolar species are all similar.

In summary, the analysis of the PCH and lifetime measurements leads to the following picture of the heterogeneity of the ground and excited states of OASS on widely different time scales. PCH was used to probe the protein on the 50-μs time scale whereas the lifetime measurements

probe the system response in the range from 1 to 10 ns. The analysis of the PCH as a function of the excitation wavelength suggests the co-presence of ketoenamine and enolimine tautomers in solution and indicates that these forms do not exchange on the PCH characteristic time scale, ~50 μs. On the other hand, the evidence of a dipolar tautomer obtained from the lifetime analysis, similarly to the single-photon excitation case, indicates that the heterogeneity of the excited state is not affected by the type of excitation used here and that the dipolar and the ketoenimine forms are in equilibrium for times of ~1–10 ns.

By counting the proteins in the excitation volume we find that of over 60 expected molecules, ~40 are not fluorescent, 15 are in the ketoenamine form, and ~5 are in the enolimine form. We identified the different forms by linking the lifetimes and the PCH parameters to the wavelength-dependent absorption properties of the tautomers. The absorption cross section of two-photon excitation estimated from the brightness, ϵ, for the ketoenamine and the enolimine tautomers show a maximum at $\lambda \cong 800$ nm and $\lambda \cong 660$ nm, respectively, with a ratio of ~1/3 in the amplitudes. According to this estimate the ratio of the ketoenamine to the enolimine tautomer cross section is inverted with respect to the case of single-photon excitation, where the ketoenamine form has a larger cross section than the enolimine one.

CONCLUSIONS

This study characterizes the spectroscopic heterogeneity of the OASS protein. By means of PCH we sample the ground-state heterogeneity through the cross section embedded in the molecular brightness ϵ. Information on the heterogeneity of the excited state is obtained from parallel measurements of the lifetime decay. With these measurements we probe the system on the nanosecond time scale and are able to detect the dipolar species, with results similar to the single-photon excitation studies. In the present case, probably due to the use of 80-MHz harmonics, the longer lifetime can only be inferred indirectly from the data. However, this is more a limit of our instrumentation than of the experimental method.

It is noteworthy that the conclusions about the number of protein tautomers in solution could not have been easily drawn from the analysis of the fluorescence correlation function, which gives the diffusion coefficients of the protein and the number of molecules per excitation volume. As a matter of fact, the diffusion coefficients of the different OASS-PLP tautomers are expected to be very similar and well within the experimental uncertainties on the determination of diffusion constants from the autocorrelation analysis. Therefore, the different tautomers could not be distinguished by means of an autocorrelation analysis of the fluorescence fluctuations. Moreover, the statistical uncertainty on the autocorrelation functions for this dim-fluorescent protein is much larger than the one affecting the PCHs.

These studies on the heterogeneity of the OASS spectroscopic states will be further extended to fluorescence anisotropy measurements on diluted protein solutions and on single proteins embedded in silica gels to detect finer heterogeneity effects of this protein system, possibly due to slightly different conformations.

We are extremely thankful to Dr. Paul F. Cook for the gift of *O*-acetylserine sulfhydrylase A-isozyme and for critical reading of the manuscript. We thank Prof. Sara Benci for helpful comments throughout this work and Dr. Marisa Huertas de la Torre for the computation of the diffusion coefficient of *O*-acetylserine sulfhydrylase.

This work has been supported by funds from the Italian Research Council (98.01117.CT14 to A.M.) and Italian Ministry of University and Scientific and Technological Research (PRIN99 to A.M.) and by funds from the National Institute for the Matter Physics (INFM), Pais-SingMol (to G.C.).

REFERENCES

Aragon, S. R., and R. Pecora. 1976. Fluorescence correlation spectroscopy as a probe of molecular dynamics. *J. Chem. Phys.* 64:1791–1803.

Arrio-Dupont, M. 1970. Etude par fluorescence de bases de Schiff du pyridoxal, comparaison avec la L-aspartate-aminotransferase. *Photochem. Photobiol.* 12:297–315.

Becker, M. A., N. M. Kredich, and G. M. Tomkins. 1969. Purification and characterization of cysteine synthetase, a bifunctional protein complex, from *Salmonella typhimurium. J. Biol. Chem.* 244:2418–2427.

Beechem, J. M., and E. Gratton. 1988. Fluorescence spectroscopy data analysis environment: a second generation global analysis program. *In* Time Resolved Laser Spectroscopy in Biochemistry, J. R. Larowicz, ed. *SPIE Proc.* 909:70–81.

Benci, S., S. Vaccari, A. Mozzarelli, and P. F. Cook. 1999. Time-resolved fluorescence of *O*-acetylserine sulfhydrylase. *Biochim. Biophys. Acta.* 1429:317–330.

Berland, K. M., P. T. So, Y. Chen, W. W. Mantulin, and E. Gratton. 1996. Scanning two-photon fluctuation correlation spectroscopy: particle counting measurements for detection of molecular aggregation. *Biophys. J.* 71:410–420.

Bieschke, J., A. Giese, W. Schulz-Schaeffer, I. Zerr, S. Poser, M. Eigen, and H. Kretzschmar. 2000. Ultrasensitive detection of pathological prion protein aggregates by dual-color scanning for intensely fluorescent targets. *Proc. Natl. Acad. Sci. U.S.A.* 97:5468–5473.

Burkhard, P., G. S. J. Rao, E. Hohenester, K. D. Schnackerz, P. F. Cook, and J. N. Jansonius. 1998. Three-dimensional structure of *O*-acetylserine sulfhydrylase from *Salmonella typhimurium. J. Mol. Biol.* 282:121–133.

Chandrasekhar, S. 1943. Stochastic problems in physics and astronomy. *Rev. Mod. Phys.* 15:1–89.

Chen, Y., J. D. Muller, P. T. C. So, and E. Gratton. 1999. The photon counting histogram in fluorescence fluctuation spectroscopy. *Biophys. J.* 77:553–567.

Christen, P., and D. E. Metzler. 1985. Transaminases. John Wiley and Sons, New York.

De la Torre, J. G., M. L. Huertas, and B. Carrasco. 2000. Calculation of hydrodynamic properties of globular proteins from their atomic-level structure. *Biophys. J.* 78:719–730.

Denk, W., J. H. Strickler, and W. W. Webb. 1990. Two-photon laser scanning fluorescence microscopy. *Science.* 248:73–76.

Ehrenberg, M., and R. Rigler. 1974. Rotational Brownian motion and fluorescence intensity fluctuations. *Chem. Phys.* 4:390–401.

Eid, J. S., J. D. Muller, and E. Gratton. 2000. Data acquisition card for fluctuation correlation spectroscopy allowing full access to the detected photon sequence. *Rev. Sci. Instrum.* 71:361–368.

Elson, E. L., and D. Magde. 1974. Fluorescence correlation spectroscopy. I. conceptual basis and theory. *Biopolymers.* 13:1–27.

Ermak, D. L., and J. A. McCammon. 1978. Brownian dynamics with hydrodynamic interactions. *J. Chem. Phys.* 69:1352–60.

Faeder, E. J., and G. G. Hammes. 1970. Kinetic studies of tryptophan synthetase. Interaction of substrates with the B subunit. *Biochemistry.* 9:4043–4049.

Hara, S., M. A. Payne, K. D. Schnackerz, and P. F. Cook. 1990. A rapid purification procedure and computer-assisted sulfide ion selective electrode assay for *O*-acetylserine sulfhydrylase from *Salmonella typhimurium. Protein Express. Purif.* 1:79–90.

Kallen, R. G., T. Korpela, A. E. Martell, Y. Matsushima, C. M. Metzler, D. E. Metzler, Y. V. Morozov, I. M. Ralston, F. A. Savin, Y. M. Torchinsky, and H. Ueno. 1985. Chemical and spectroscopic properties of pyridoxal and pyridoxamine phosphates. *In* Transaminases. P. Christen, and D. E. Metzler, editors. John Wiley and Sons, New York. 37–108.

Kask, P., K. Palo, N. Fay, L. Brand, Ü. Mets, D. Ullmann, J. Jungmann, J. Pschorr, and K. Gall. 2000. Two-dimensional fluorescence intensity distribution analysis: theory and applications. *Biophys. J.* 78:1703–1713.

Kask, P., K. Palo, D. Ullmann, and K. Gall. 1999. Fluorescence-intensity distribution analysis and its application in biomolecular detection technology. *Proc. Natl. Acad. Sci. U.S.A.* 96:13756–13761.

Koppel, D. E., F. Morgan, A. E. Cowan, and J. H. Carson. 1994. Scanning concentration correlation spectroscopy using the confocal laser microscope. *Biophys. J.* 66:502–507.

Levy, S., and A. Danchin. 1988. Phylogeny of metabolic pathways: *O*-acetylserine sulfhydrylase-A is homologous to the tryptophan synthase beta subunit. *Mol. Microbiol.* 2:777–783.

Magde, D., and E. L. Elson. 1974. Fluorescence correlation spectroscopy. II. An experimental realization. *Biopolymers.* 13:29–61.

Moerner, W. E., and M. Orrit. 1999. Illuminating single molecules in condensed matter. *Science.* 283:1670–1676.

Müller, J. D., Y. Chen, and E. Gratton. 2000. Resolving heterogeneity on the single molecular level with the photon-counting histogram. *Biophys. J.* 78:474–486.

Qian, H., and E. L. Elson. 1989. Characterization of the equilibrium distribution of polymer molecular weights by fluorescence distribution spectroscopy (theoretical results). *In* Applied Polymer Symposia. John Wiley and Sons, New York. 305–314.

Qian, H., and E. L. Elson. 1990. Distribution of molecular aggregation by analysis of fluctuation moments. *Proc. Natl. Acad. Sci. U.S.A.* 85: 5479–5483.

Qian, H., and E. L. Elson. 1991. Analysis of confocal laser-microscope optics for 3-D fluorescence correlation spectroscopy. *Appl. Optics.* 30: 1185–1195.

Rege, V. D., N. M. Kredich, C.-H. Tai, W. E. Karsten, K. D. Schnackerz, and P. F. Cook. 1996. A change in the internal aldimine lysine (K42) in *O*-acetylserine sulfhydrylase to alanine indicates its importance in transamination and as general base catalyst. *Biochemistry.* 35: 13485–13493.

Rigler, R., U. Mets, J. Windengren, and P. Kask. 1993. Fluorescence correlation spectroscopy with high count rate and low background: analysis of translational diffusion. *Eur. Biophys. J.* 22:169–175.

Saleh, B. 1978. Photoelectron Statistics, with Applications to Spectroscopy and Optical Communications. Springer-Verlag, Berlin.

Schnackerz, K. D., C.-H. Tai, J. W. Simmons, T. M. Jacobson, G. S. J. Rao, and P. F. Cook. 1995. Identification and spectral characterization of the external aldimine of the *O*-acetylserine sulfhydrylase reaction. *Biochemistry.* 34:12152–12160.

Tai, C.-H., S. R. Nalabolu, T. M. Jacobson, D. E. Minter, and P. F. Cook. 1993. Kinetic mechanism of the A and B isozymes of *O*-acetylserine sulfhydrylase from *Salmonella typhymurium* LT-2 using the natural and alternative reactants. *Biochemistry.* 32:6433–6442.

Tanford, C. 1961. Physical Chemistry of Macromolecules. Wiley, New York.

Tsien, R. Y., and Y. Wagonner. 1995. Fluorophores for Confocal Microscopy, Vol. 2. Plenum Press, New York. 267–277.